

Transport properties of a multichannel Kondo dot in a magnetic field

Christoph B. M. Horig and Dirk Schuricht

*Institute for Theory of Statistical Physics, RWTH Aachen, 52056 Aachen, Germany and
JARA-Fundamentals of Future Information Technology*

(Dated: April 5, 2012)

We study the nonequilibrium transport through a multichannel Kondo quantum dot in the presence of a magnetic field. We use the exact solution of the two-loop renormalization group equation to derive analytical results for the g factor, the spin relaxation rates, the magnetization, and the differential conductance. We show that the finite magnetization leads to a coupling between the conduction channels which manifests itself in additional features in the differential conductance.

PACS numbers: 73.63.-b, 71.10.-w, 05.70.Ln, 05.10.Cc

Introduction.—The study of a localized spin coupled via an antiferromagnetic exchange interaction J to K independent electronic reservoirs has a long history in condensed matter physics.¹ In the simplest case of $K = 1$ the electron spins completely screen the local spin at low energies and thus lead to a Fermi liquid. In a renormalization group (RG) analysis this situation is characterized by the divergence of the renormalized exchange coupling $J(\Lambda)$ at the Kondo scale $\Lambda = T_K$. The situation is completely changed² if the spin is coupled to more than one screening channel ($K > 1$). Then the renormalized exchange coupling stays finite and flows to a non-trivial fixed point^{2,3} $J^* \sim 1/K$ at low energies, which manifests itself in unusual non-Fermi liquid behavior like a non-integer “ground-state degeneracy” or characteristic power laws in various observables.^{4,5}

The recent developments in the ability to engineer devices on the nanoscale lead to the experimental realization⁶ of two-channel Kondo physics in a quantum dot set-up.⁷ In this set-up it was possible to measure the differential conductance and observe universal scaling and square-root behavior which are characteristic for the two-channel Kondo effect. This triggered theoretical studies^{8–10} of the transport properties of multichannel systems using conformal field theory as well as numerical and perturbative RG methods. The latter uses a perturbative expansion in the renormalized exchange coupling which is well-controlled provided $K \gg 1$. Specifically, Mitra and Rosch⁹ calculated the differential conductance, the splitting of the Kondo resonance in the T matrix, and the current-induced decoherence in the absence of a magnetic field. Recently the spin dynamics was studied¹⁰ in the absence of a bias voltage and shown to possess pure power-law decay with an exponent $g = 4/K$.

In this Brief Report we extend the analysis of Mitra and Rosch⁹ to include an external magnetic field. We perform a real-time RG (RTRG) analysis¹¹ to derive the renormalized magnetic field, the spin relaxation rates, the magnetization of the quantum dot, and the current. In particular, we focus on inelastic cotunneling processes which lead to characteristic features in the differential conductance whenever one of the applied bias voltages V_i ’s equals the value of the renormalized magnetic field. We further show that the finite magnetization on the

dot leads to a coupling of the conduction channels which results in additional features in the differential conductance.

Model.—We consider a quantum dot possessing a spin-1/2 degree of freedom, which is coupled via an exchange interaction J to K independent electronic reservoirs. At low energies each reservoir constitutes one screening channel for the local spin thus leading to an over-screened situation for $K > 1$. We will thus use the terms reservoir and channel interchangeably. Furthermore, the spin-1/2 is subject to an external magnetic field h_0 . Each reservoir consists of a left (L) and right (R) lead which are held at chemical potentials μ_α^i , $\alpha = L, R$, $i = 1, \dots, K$ (see Fig. 1). Specifically we consider the system

$$H = \sum_{i\alpha k\sigma} \epsilon_k c_{i\alpha k\sigma}^\dagger c_{i\alpha k\sigma} + h_0 S^z + \frac{J_0}{2\nu_0} \sum_{i\alpha\alpha'kk'\sigma\sigma'} \vec{S} \cdot \vec{\sigma}_{\sigma\sigma'} c_{i\alpha k\sigma}^\dagger c_{i\alpha'k'\sigma'} \quad (1)$$

Here $c_{i\alpha k\sigma}^\dagger$ and $c_{i\alpha k\sigma}$ create and annihilate electrons with momentum k and spin $\sigma = \uparrow, \downarrow$ in lead α of the reservoir i , $\vec{\sigma}$ denotes the Pauli matrices, and \vec{S} is the spin-1/2 operator on the dot. The antiferromagnetic exchange coupling $J_0 > 0$ is dimensionless in our convention. We stress that the exchange term does not couple differ-

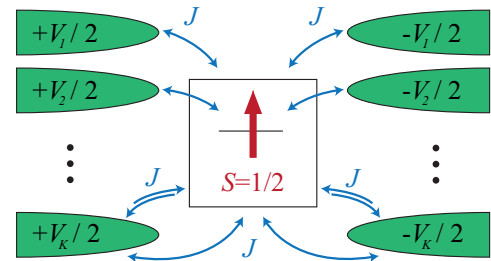


FIG. 1. (Color online) Sketch of the K -channel Kondo model (1). The channels are labeled by $i = 1, \dots, K$, each channel is decomposed into two leads $\alpha = L, R$ held at chemical potentials $\mu_{L/R}^i = \pm V_i/2$. The spin-1/2 on the dot is subject to a magnetic field h_0 . The exchange interaction J between dot and leads present in all channels is depicted for the K th channel explicitly.

ent reservoirs. The chemical potentials in the leads are parametrized by $\mu_{L/R}^i = \pm V_i/2$ thus applying a bias voltage V_i to each reservoir. Furthermore we introduce an ultra-violet cutoff D in each reservoir via the density of states $N(\omega) = \nu_0 D^2/(D^2 + \omega^2)$. In the absence of a magnetic field the transport properties of the model (1) have been previously studied in Ref. 9.

RG analysis.—Following Ref. 11 we have performed a two-loop RTRG analysis including a consistent derivation of the relevant relaxation rates. This method has been successfully applied to study transport properties of other Kondo-type quantum dots in the past.^{11,12} The starting point is an RG equation for the renormalized exchange coupling $J(\Lambda)$ obtained by integrating out the high-energy degrees of freedom in the reservoirs. To accomplish this the one introduces a cutoff Λ into the Fermi function and integrates out the Matsubara poles on the imaginary axis by decreasing the cutoff from its initial value $\Lambda_0 \sim D$ down to some physical energy scale. The RG equation for the K -channel model (1) reads up to two loop

$$\Lambda \frac{d}{d\Lambda} J = \beta(J) = -2J^2(1 - KJ), \quad (2)$$

which defines the reference solution $J(\Lambda)$ for our analysis. The RG flow has the well-known² non-trivial fixed point $J^* = 1/K$. The scaling dimension of the leading irrelevant operator is $\Delta = \beta'(J^*) = 2/K$, which is valid for $K \gg 1$ while the exact result is given by⁵ $\Delta = 2/(K+2)$. The RG equation possesses the invariant

$$T_K = \Lambda_0 \left(\frac{eJ_0}{J^* - J_0} \right)^{K/2} e^{-1/2J_0}, \quad (3)$$

which defines the Kondo temperature. With the initial condition $J_0 = J(\Lambda_0)$ the solution of the RG equation can be explicitly written as

$$J(\Lambda) = \frac{J^*}{1 + W(z)}, \quad z = \left(\frac{\Lambda}{T_K} \right)^\Delta. \quad (4)$$

Here $W(z)$ denotes the Lambert W function¹³ defined by $z = W(z)e^{W(z)}$, which satisfies $W'(z) = W(z)/z/(1 + W(z))$ for $z \neq 0$. The fixed point J^* is reached for $\Lambda \rightarrow 0$ as $W(0) = 0$. We note that the solution (4) is valid for all J_0 but, of course, the derivation of (2) requires $J_0 \ll 1$. If $J_0 < J^*$ we can perform the scaling limit $\Lambda_0 \rightarrow \infty$ and $J_0 \rightarrow 0$ while keeping the Kondo temperature constant. In this limit the solution for $\Lambda \ll T_K$ simplifies to

$$J(\Lambda) = J^* \left[1 - \left(\frac{\Lambda}{T_K} \right)^\Delta \right], \quad (5)$$

i.e. there is a characteristic power-law behavior. Observables are calculated in a systematic expansion around the reference solution and can be expressed in terms of the

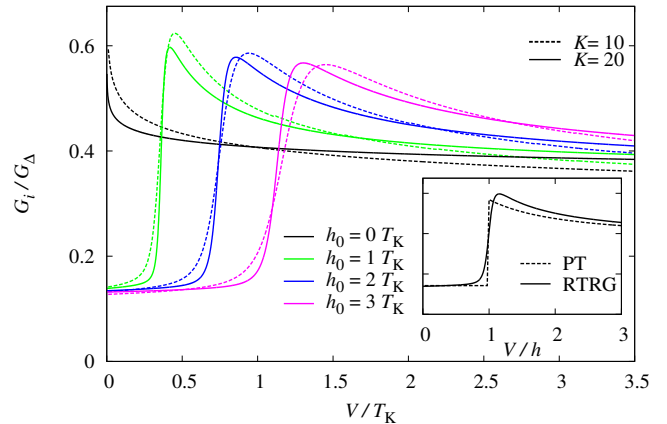


FIG. 2. (Color online) Differential conductance of an individual channel for identical bias voltages $V_i = V$ and $K = 10$ (dashed lines) or $K = 20$ (solid lines) channels. We use the normalization $G_\Delta = (\frac{2e^2}{h}) \frac{3\pi^2}{16} \Delta^2$. For zero field one finds⁹ $G/G_\Delta = 1 - 2(V/T_K)^\Delta$, *i.e.* $G/G_\Delta \rightarrow 1$ for $V \rightarrow 0$. Inset: Comparison of RTRG (solid line) and renormalized perturbation theory (PT) up to $\mathcal{O}(J_c^2)$ (dashed line) for $h_0 = T_K$ and $K = 20$. We note that the broadening of the feature at $V = h$ is not captured in PT.

renormalized exchange coupling $J_c \equiv J(\Lambda_c)$ at the physical energy scale¹⁴ (we consider $T = 0$)

$$\Lambda_c = \max\{V, h_0\}. \quad (6)$$

In contrast to the one-channel Kondo model the existence of the attractive fixed point $J^* = 1/K$ implies that this expansion is well-defined for all Λ_c provided $K \gg 1$. We have calculated the effective dot Liouvillian and the current kernel yielding the renormalized magnetic field, the spin relaxation rates, the dot magnetization, and the current including the leading logarithmic corrections. All calculations follow Ref. 11, we present here only the results and discuss their properties.

Identical bias voltages.—First let us assume that all bias voltages are identical, *i.e.* $V_i = V$. Straightforward calculation yields the renormalized magnetic field

$$h = [1 - K(J_c - J_0)]h_0, \quad (7)$$

which gives for the g factor in leading order (we consider the scaling limit $J_0 \rightarrow 0$ from now)

$$g = 2 \frac{\partial h}{\partial h_0} = 2(1 - KJ_c)^{\Lambda_c \ll T_K} 2 \left(\frac{\Lambda_c}{T_K} \right)^\Delta. \quad (8)$$

The longitudinal and transverse spin relaxation rates

$$\Gamma_1 = \pi \left[h + \frac{1}{2}(|V - h|_2 + V + h) \right] KJ_c^2, \quad (9)$$

$$\Gamma_2 = \frac{\pi}{2} \left[V + h + \frac{1}{2}(|V - h|_1 + V + h) \right] KJ_c^2, \quad (10)$$

with

$$|x|_l = \frac{2}{\pi} x \arctan \frac{x}{\Gamma_l}, \quad l = 1, 2. \quad (11)$$

We note that for $\Lambda_c \gg T_K$ the renormalization of the magnetic field (7) is much stronger than in the one-channel Kondo model, as the spin on the dot is coupled to more screening channels.

Explicit formulas for the dot magnetization and the current are given in Eq. (14) below for the case of different bias voltages. Simplifying to $V_i = V$ we obtain the differential conductance $G_i = dI_i/dV_i$ per channel, which is plotted in Fig. 2. The conductance sharply increases around $V = h$ where inelastic cotunneling processes start to contribute. Due to the strong renormalization of the magnetic field the increase occurs at voltages much smaller than the applied magnetic field h_0 . Close to the resonance we find

$$G_i = \begin{cases} \frac{\pi}{4} J_c^2 [1 + 2J_c \mathcal{L}_2(V - h)] & \text{for } V < h, \\ \pi J_c^2 [1 + 2\pi J_c \mathcal{L}_2(V - h)] & \text{for } V > h, \end{cases} \quad (12)$$

where we assumed $|V - h| \ll h$ and defined

$$\mathcal{L}_l(x) = \ln \frac{\Lambda_c}{\sqrt{x^2 + \Gamma_l^2}}, \quad l = 1, 2. \quad (13)$$

We note that (12) is formally identical to the differential conductance in the one-channel Kondo model¹¹ except for the functional form of the renormalized coupling (5). In particular, there is no explicit dependence on the number of channels. We further note that close to the fixed point the conductance (12) is a quantity of order $1/K^2$. The logarithmic divergencies at $V = h$ are cut off by the transverse spin relaxation rate Γ_2 . Thus, as $\Gamma_2 \sim 1/K$, this feature becomes sharper with increasing K . At small voltages $V < h$ the conductance is independently of the bias voltage given by $G_i = \pi J_c^2/4$. In particular, a power-law behavior in the voltage is only found for vanishing magnetic field⁹ while (5) yields a power-law dependence on the magnetic field. In the limit of a large field $h \gg T_K$ the linear conductance can be derived using¹³ $W(z) \sim \ln z$ for $z \rightarrow \infty$ to be $G_i(V = 0, h) = \pi/16/\ln^2(h/T_K)$, which is identical to the result in the one-channel model.

Different bias voltages.—In the following we relax the condition $V_i = V$ and consider channel-dependent bias voltages V_i . This introduces further energy scales which will give rise to additional features in the dot magnetization and thus the differential conductance. In this general set-up the magnetization and current through the i th channel are given by

$$M = -\frac{f_1}{2f_2}, \quad I_i = f_I^i + 2M f_M^i \quad (14)$$

where $f_{1,2}$ denote rates appearing in the Liouvillian and $f_{I,M}^i$ are similar terms in the current kernel. Explicitly

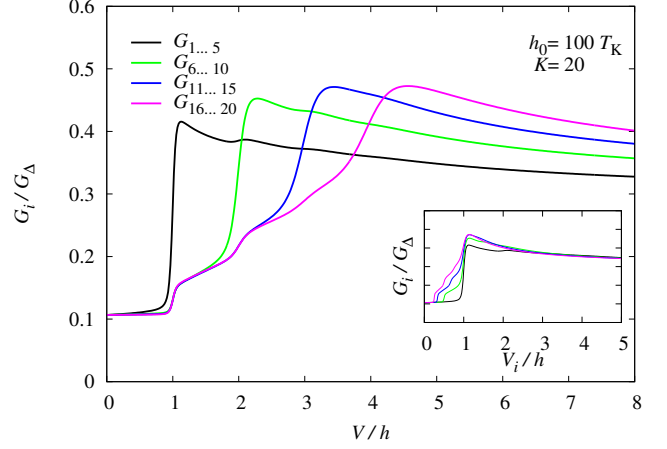


FIG. 3. (Color online) Differential conductance G_i through channel i for $h_0 = 100 T_K$ and $K = 20$. The bias voltages are applied such that series of five channels have identical voltages, *i.e.* $V_i = a_i V$ with $a_{1,\dots,5} = 1$, $a_{6,\dots,10} = 1/2$, $a_{11,\dots,15} = 1/3$, and $a_{16,\dots,20} = 1/4$. For $h_0 = 0$ the conductance is similar to the black curve in Fig. 2, *i.e.* there are no features. Inset: Same situation as in the main panel, but plotted with respect to the respective bias voltage V_i .

these rates read

$$f_1 = 2\pi K J_c^2 h + 4\pi K J_c^3 h \mathcal{L}_2(h) - 2\pi J_c^3 \sum_{j=1\dots K} (V_j - h) \mathcal{L}_2(V_j - h), \quad (15)$$

$$f_2 = \pi K J_c^2 h + 2\pi K J_c^3 h \mathcal{L}_2(h) + \frac{\pi}{2} J_c^2 \sum_{j=1\dots K} (|V_j - h|_2 + V_j + h) + \pi J_c^3 \sum_{j=1\dots K} (|V_j - h|_2 - V_j + h) \mathcal{L}_2(V_j - h), \quad (16)$$

$$f_I^i = \frac{3}{4} \pi J_c^2 V_i + \pi J_c^3 V_i \mathcal{L}_1(V_i) + \pi J_c^3 (V_i - h) \mathcal{L}_2(V_i - h), \quad (17)$$

$$f_M^i = -\frac{\pi}{4} J_c^2 (|V_i - h|_2 - V_i - h) + \pi J_c^3 V_i \mathcal{L}_1(V_i) + \pi J_c^3 h \mathcal{L}_2(h) - \frac{\pi}{2} J_c^3 |V_i - h|_2 \mathcal{L}_2(V_i - h). \quad (18)$$

The relaxation rates for the case of different bias voltages are obtained by straightforward generalization of Eqs. (9) and (10). In the derivation of Eqs. (15)–(18) we have neglected all terms in order J_c^3 that do not contain logarithms at either $h = 0$, $V = 0$, or $V = h$. Thus when calculating the magnetization one has to expand consistently up to this order.

We stress that although the different channels are not directly coupled via exchange interactions, the finite magnetization M mediates a feedback between them. Consider for example the differential conductance of channel 1, *i.e.* the black curve in Fig. 3. The sharp increase at $V = V_1 = h$ is again due to the onset of inelastic cotunneling processes. However, there is a second feature at $V \approx 2h$ which is caused by the non-trivial voltage de-

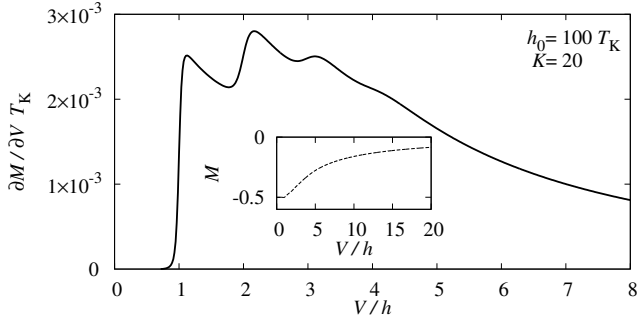


FIG. 4. Derivative of the magnetization with respect to the voltage, *i.e.* $\partial M/\partial V$. All parameters are as in Fig. 3. We observe pronounced features at $V = h$ and $V = 2h$. Inset: Magnetization as a function of the bias voltage.

pendence of the dot magnetization. This can be seen in the derivative $\partial M/\partial V$ shown in Fig. 4, which directly enters the differential conductance [see (14)]. Similarly, the conductance in channel 6 (green curve in Fig. 3) possesses a feature at $V = 2V_6 = h$ which is caused by the effect of the applied voltage in channels 1 to 5 onto M , while the increase at $V_6 = h$ (*i.e.* $V = 2h$) is due to the onset of inelastic cotunneling in channel 6. In this way the nonequilibrium magnetization introduces additional features into the individual conductances. We stress that such coupling effects between the channels are absent for vanishing magnetic field⁹ or if all applied bias voltages are identical (see Fig. 2).

As a special case of the general set-up with channel-dependent bias voltages we can recover the experimental situation realized⁶ by Potok *et al.* in a semicon-

ductor quantum dot. This is achieved by setting the chemical potentials to $\mu_{L/R}^1 = \pm V/2$ and $\mu_{L/R}^i = 0$ for $i = 2, \dots, K$. In each of the channels $2, \dots, K$ we introduce even and odd combinations of the electron operators, $(c_{iLk\sigma} \pm c_{iRk\sigma})/\sqrt{2}$, such that the even combinations couple to the spin on the dot with exchange interaction $2J$ while the odd ones decouple completely. The resulting RG equation for J is given by (2) and thus possesses the fixed point J^* . The experimental set-up⁶ is now obtained by specializing to $K = 2$. In the presence of a magnetic field the resulting differential conductance is very similar to the case of identical bias voltages shown in Fig. 2. In particular, since the second channel does not provide an additional energy scale there appear no features in the differential conductance beside the cotunneling peak at $V = h$. A possible experimental set-up to observe the additional features shown in Fig. 3 thus requires at least two channels with non-zero and different bias voltages.

Conclusions.—To sum up, we have studied the nonequilibrium transport properties of a multichannel Kondo quantum dot in the presence of a magnetic field. We used the solution of the two-loop RG equation to derive analytical results for the g factor, the spin relaxation rates, the dot magnetization, and the differential conductance. The latter shows typical features of inelastic cotunneling. We showed that the main difference to the previously studied⁹ situation without magnetic field is the appearance of additional features in the differential conductance, which originate in the feedback between the channels mediated by the finite dot magnetization.

We thank S. Andergassen, A. Rosch, and H. Schoeller for useful discussions. This work was supported by the German Research Foundation (DFG) through the Emmy-Noether Program.

¹ A. C. Hewson, *The Kondo Problem to Heavy Fermions* (Cambridge University Press, Cambridge, 1993).

² P. Nozières and A. Blandin, *J. Phys. France* **41**, 193 (1980).

³ J. Gan, N. Andrei, and P. Coleman, *Phys. Rev. Lett.* **70**, 686 (1993); J. Gan, *J. Phys.: Condens. Matter* **6**, 4547 (1994).

⁴ N. Andrei and C. Destri, *Phys. Rev. Lett.* **52**, 364 (1984); A. M. Tsvelick and P. B. Wiegmann, *Z. Phys. B* **54**, 201 (1984); I. Affleck and A. W. W. Ludwig, *Phys. Rev. Lett.* **67**, 161 (1991).

⁵ A. W. W. Ludwig and I. Affleck, *Phys. Rev. Lett.* **67**, 3160 (1991); I. Affleck and A. W. W. Ludwig, *Phys. Rev. B* **48**, 7297 (1993).

⁶ R. M. Potok, I. G. Rau, H. Shtrikman, Y. Oreg, and D. Goldhaber-Gordon, *Nature (London)* **446**, 167 (2007).

⁷ Y. Oreg and D. Goldhaber-Gordon, *Phys. Rev. Lett.* **90**, 136602 (2003).

⁸ A. I. Tóth, L. Borda, J. von Delft, and G. Zaránd, *Phys. Rev. B* **76**, 155318 (2007); R. Žitko and J. Bonča, *ibid.* **77**, 245112 (2008); E. Sela and I. Affleck, *Phys. Rev. Lett.* **102**, 047201 (2009); E. Vernek, C. A. Büsler, G. B. Martins, E. V. Anda, N. Sandler, and S. E. Ulloa, *Phys. Rev. B*

80, 035119 (2009); A. K. Mitchell and D. E. Logan, *ibid.* **81**, 075126 (2010); E. Sela, A. K. Mitchell, and L. Fritz, *Phys. Rev. Lett.* **106**, 147202 (2011); A. K. Mitchell, D. E. Logan, and H. R. Krishnamurthy, *Phys. Rev. B* **84**, 035119 (2011); A. K. Mitchell, E. Sela, and D. E. Logan, *Phys. Rev. Lett.* **108**, 086405 (2012); A. K. Mitchell and E. Sela, e-print arXiv:1203.4456.

⁹ A. Mitra and A. Rosch, *Phys. Rev. Lett.* **106**, 106402 (2011).

¹⁰ M. Pletyukhov and H. Schoeller, e-print arXiv:1201.6295.

¹¹ H. Schoeller, *Eur. Phys. J. Special Topics* **168**, 179 (2009); H. Schoeller and F. Reininghaus, *Phys. Rev. B* **80**, 045117 (2009); *ibid.* **80**, 209901(E) (2009).

¹² D. Schuricht and H. Schoeller, *Phys. Rev. B* **80**, 075120 (2009); M. Pletyukhov, D. Schuricht, and H. Schoeller, *Phys. Rev. Lett.* **104**, 106801 (2010); M. Pletyukhov and D. Schuricht, *Phys. Rev. B* **84**, 041309(R) (2011); C. B. M. Hørig, D. Schuricht, and S. Andergassen, *ibid.* **85**, 054418 (2012).

¹³ R. M. Corless, G. H. Gonnet, D. E. G. Hare, D. J. Jeffrey, and D. E. Knuth, *Adv. Comput. Math.* **5**, 329 (1996).

¹⁴ For the numerical evaluation we use $\Lambda_c = \sqrt{V^2 + h_0^2}$.